International Journal of Biological Macromolecules 158 (2020) 251–257

Contents lists available at ScienceDirect

International Journal of Biological Macromolecules

journal homepage: http://www.elsevier.com/locate/ijbiomac

Nanoformulation of fibrinogen by thermal stabilization of its electrostatic complexes with hyaluronic acid

Eleni Vlassi, Aristeidis Papagiannopoulos *

Theoretical and Physical Chemistry Institute, National Hellenic Research Foundation, 48 Vassileos Constantinou Avenue, 11635 Athens, Greece

ARTICLE INFO

Article history:
Received 27 March 2020
Received in revised form 26 April 2020
Accepted 27 April 2020
Available online 1 May 2020

Keywords:
Fibrinogen
Polysaccharide-protein nanoparticles
Thermal treatment
Light scattering
Hyaluronic acid
Curcumin

ABSTRACT

The formulation of well-defined and stable fibrinogen-based nanoparticles (NPs) without the use of any chemical reaction or any toxic organic solvent is reported. Electrostatic interaction between hyaluronic acid (HA) and fibrinogen (Fbg) leads to well-defined complexes at acidic pH which however readily dissolve at neutral pH. On the other hand, when thermal treatment is applied on the pre-formed complexes NPs keep their integrity. Circular dichroism indicates that the protein's native secondary conformation in the final NPs is not affected by the formulation. The tendency of the complexes to aggregate at elevated ionic strengths is greatly suppressed after the application of the temperature treatment protocol. This characteristic is even more pronounced at neutral pH and it is connected to the enhanced surface charge of the NPs. The encapsulation of the hydrophobic compound curcumin causes only weak secondary aggregation. This work shows that the ability of Fbg to self-assemble upon thermal treatment can be effectively used to stabilize Fbg nanoformulations inside complexes with polysaccharides.

1. Introduction

Protein NPs offer biocompatibility, biodegradability and nontoxicity and therefore are attractive for the delivery of pharmaceuticals and nutraceuticals [1,2]. Fabrication of protein NPs is normally achieved by emulsion-solvent evaporation [3], desolvation [4], coacervation [5] and electrospraying [6] methods. In addition proteins have been used in NPs in order to modify the nanoparticle/biological fluid interface for targeted delivery in tumors [7], to test the ability to treat fibrosis conditions [8] and diagnostic purposes [9]. They can create superstructures with controllable size and charge, by spontaneous incorporation in self-assembled micelles [10,11] and in complexes with oppositely charged polyelectrolytes [12,13], or more specifically, with polysaccharides [14]. However, electrostatic complexation is prone to instability upon pH changes. Thermal treatment of polysaccharide/protein complexes has been proposed for their stabilization [15,16], in a method that takes advantage of the unfolding of hydrophobic residues and the formation of irreversible protein-protein bridges upon temperature increase [17]. Encapsulation of hydrophobic compounds has been already achieved in β-lactoglobulin/polysaccharide [18,19] and in chondroitin sulfate (CS)/bovine serum albumin (BSA) complexes stabilized by thermal treatment [20].

Fbg is a blood protein that plays a critical role in blood clotting and aggregation of platelets and in the interaction of blood with biomaterials [21,22]. It is also an effective agent in wound healing and tissue engineering applications because it has active sites that are able to bind fibroblasts, endothelial cells and their growth factors [23]. Hydrogels with good cytocompatibility have been assembled by knob-hole interaction between Fbg and HA. The polysaccharide was grafted with knob-peptides that could specifically couple with Fbg [24]. Nano- and micro- structured biomaterials based on Fbg are promising as carriers of biomolecules, drugs and gene [25]. Fbg has been shown to stabilize nutraceutical compounds, such as curcumin, in aqueous solutions [26]. Synthesis of non-toxic Fbg NPs by the aid of calcium chloride in a two-step coacervation method has been reported [27]. These Fbg NPs when loaded with curcumin were additionally found to be effective for cancer treatment with low cytotoxicity in healthy cells [28]. Nanogels of Fbg that was grafted with a thermoresponsive polymer have shown promising results as drug carriers for breast cancer therapy [29].

In this work we use electrostatic complexation between HA and Fbg in order to produce well-defined complexes in acidic conditions. We perform a thermal treatment protocol in order to stabilize the complexes into NPs. The distributions of sizes in solution and the molar mass and radius of gyration of the complexes and NPs at different pH and ionic strengths are measured by light scattering while the protein conformation is quantified by circular dichroism. Loading the hydrophobic bioactive compound curcumin is tested in terms of its effect on NPs size and mass. This study offers a versatile and biocompatible methodology for the synthesis of NPs based on Fbg for their use in drug delivery and tissue engineering applications.

* Corresponding author.
E-mail address: apapagiannopoulos@eie.gr (A. Papagiannopoulos).

https://doi.org/10.1016/j.ijbiomac.2020.04.244
0141-8130/

2. Materials and methods

2.1. Materials and sample preparation

Fibrinogen (Fbg) and curcumin were purchased from Sigma. Sodium salt hyaluronic acid (HA) with M = 5000 gmol^{-1} (PDI ~ 1.5) was a kind gift from Uni-Pharma (Greece). All components were used as received. Aqueous stock solutions of HA were prepared at the concentration 1.0 mgml^{-1} in distilled water and were left overnight to equilibrate at 4 °C. Fbg stock solutions at the concentration 10 mgml^{-1} were prepared by disolving Fbg powder in saline solution at 37 °C. Proper volumes of stock solutions, distilled water and citric acid (CA) were mixed under stirring to obtain HA-Fbg complexes. Water was first mixed with CA solution (1 M) in minor quantities to fix pH at the desired acidic conditions, HA solution was subsequently added and Fbg solution was finally introduced. Experiments were performed on four different HA/Fbg mixtures with HA concentration at 3, 5, 7 and 9 × 10^{-3} mgml^{-1} and Fbg contration at 0.1 mgml^{-1}. Minor quantities of NaOH (1 M) were used for experiments at neutral pH. Temperature treatment was performed by placing sealed vials of HA-Fbg complexes in solution in an oven at 85 °C for 20 min and cooling at room temperature afterwards. Salt concentration was fixed by introducing the desired volume 1 M NaCl. To load the bioactive compound, curcumin was dispersed in ethanol (36.84 × 10^{-3} mgml^{-1} or 100 μM) and 10 μl from this dispersion were added to 1 ml of NP solution. The concentration of curcumin in the final solutions was 1 μM. The curcumin/Fbg molar ratio was 0.34, which is near the ratio 0.5 that has been used by others [26]. Mixtures were left for the ethanol to evaporate in a fume cupboard and were gently shaken for 48 h at room temperature. All experiments were performed at 25 °C.

2.2. Light scattering

An ALV system (ALV-CG-3 goniometer/ALV-5000/EPP multi tau digital correlator) with a He—Ne laser (λ = 632.8 nm) was used for light scattering (LS) experiments. The Rayleigh ratio $R(q)$ for static light scattering (SLS) [30] is collected in order to measure the weight-average molar mass M and the form factor $P(q)$ of the scattering particles (Eq. (1)).

$$\frac{Kc}{R(q)} = \frac{1}{MP(q)} \tag{1}$$

Where c is the mass concentration of the scattering particles in solution and q is scattering wave vector ($q = \frac{4\pi n_0}{\lambda} sin\frac{\theta}{2}$). The contrast factor for LS is $K = \frac{4\pi^2 n_0^2}{N_A \lambda^4}(\partial n/\partial c)^2$ with n_0 is the solvent's refractive index and $\partial n/\partial c$ the refractive index increment of the scattering particles in the specific solvent. We used $\frac{\partial n}{\partial c} = 0.18\ ml/g$ which is near the values of both HA and Fbg.

$$\frac{R(q)}{Kc} = M \cdot e^{-\frac{1}{3}q^2R_g^2} + B \cdot (q^2)^2 \tag{2}$$

In the Guinier approximation the form factor is $P(q) = e^{-\frac{1}{3}q^2R_g^2}$ and it provides the radius of gyration R_g of the scattering particles. A quadratic approximation (in q^2) for the form factor (Eq. (2)) so that the whole series of Guinier plots [20,31] could be fitted at the whole q range (see Results and Discussion).

In dynamic light scattering [32] (DLS) the autocorrelation functions of scattered light intensity $g_2(\tau)$ as a function of lag-time τ lead to the field autocorrelation functions $g_1(\tau)$ using the Siegert relation $g_2(\tau) - 1 = \beta|g_1(\tau)|^2$ (β is a normalization constant). The characteristic relaxation time τ_c(q) of $g_1(\tau)$ was extracted by cumulant analysis. The characteristic relaxation rate $\Gamma(q) = 1/\tau_c(q)$ can be modelled by Eq. (3) where D_0 is the diffusion coefficient q = 0 and C is a constant.

$$\Gamma(q) = D_0 \cdot q^2 + C \cdot (q^2)^2 \tag{3}$$

CONTIN analysis was used to extract the distribution of relaxation times $f(\tau)$. Stokes-Einstein relation (Eq. (4)) leads to the hydrodynamic radius R_h (η is the solvent viscosity and D the diffusion coefficient) and is also used to transform the distribution of relaxation times to the distribution of hydrodynamic radii $f(R_h)$ by $D = 1/\tau q^2$. In this work R_h values are reported based on CONTIN analysis at θ = 90°, while $\Gamma(q)$ plots are shown only to discuss the angular dependence of the relaxation rate.

$$R_h = \frac{k_B T}{6\pi\eta D} \tag{4}$$

SLS and dynamic DLS data were collected over a wide angular range from θ = 30° to θ = 130°.

2.3. Electrophoretic light scattering

Electrophoretic light scattering (ELS) was performed on a Zetasizer Nano-ZS (Malvern Instruments Ltd). Zeta potential (ζ_p) was calculated with the Henry equation under the Smoluchowski approximation. Averages of 10 measurements taken at scattering angle θ = 173° are reported.

2.4. Circular dichroism

Experiments with circular dichroism (CD) were performed on a Jasco J-815 CD spectrophotometer while the aqueous solutions were loaded into suprasil quartz cells (1 mm). CD spectra from every sample were accumulated as averages of 4 successive measurements. Secondary structure was analysed by the BeStSel software [33].

2.5. UV–visible spectroscopy

A UV–vis-NIR spectrophotometer Perkin-Elmer (Lamda 19) was used for UV–vis absorption spectroscopy. Samples were loaded in a 1-cm-long quartz cuvette. The absorbance was recorded from 300 to 600 nm in order to obtain the characteristic absorption spectrum of curcumin.

3. Results and discussion

3.1. Electrostatic complexation between HA and Fbg

Polysaccharide-protein complexation has been traditionally utilized either by mixing the two components at different mass ratios at a certain pH or changing the pH while the mass ratio of the two components is fixed [34–36]. Turbidity measurements are often employed to monitor complexation and coacervation. As in our previous work [20] we use light scattering as a sensitive probe of size and molar mass in dilute solutions and apply mixing of the components at a fixed pH.

Fbg has an isoelectric point pI = 5.8, a net charge of about −8 at physiological conditions i.e. pH ~ 7.4 and a net charge of about +20 at pH 4 [37]. We performed mixing of the two components at pH 4 where Fbg is positive and is strongly attracted to HA. Strong complexation between charged macromolecules is expected at the point of stoichiometric neutrality conditions in the bulk solution [36]. HA carries one negative charge per sugar pair. The charge ratio of negative to positive charges in solution is calculated by $\frac{[-]}{[+]} = \frac{c_{HA}/M_{HA} \cdot Z_{HA}}{c_{Fbn}/M_{Fbn} \cdot Z_{Fbn}}$, where c_i, M_i and Z_i are the mass concentration, molar mass and net absolute

charge of the components (i = HA -disaccharide unit or Fbg) respectively. Charge neutrality of HA-Fbg mixtures at pH ~ 4 is expected at $\frac{c_{HA}}{c_{Fbn}} \approx 0.023$. In this work we report on results from $\frac{c_{HA}}{c_{Fbn}}$ ratios in the range 0.03–0.09 where strong complexation leading to well-defined complexes of high molar mass is observed. The concentration of Fbg was chosen so that the resulting solutions of complexes were still transparent for the LS experiments.

HA-Fbg NPs in aqueous solutions were characterized by DLS and SLS in order to examine the size distributions (presence of single or multiple size populations) and measure the molar mass of the complexes. Single populations with relatively narrow distribution are found for all HA contents in the acidic solutions. In Fig. 1a CONTIN analysis examples from HA-Fbg complexes at different concentrations of HA are shown. In the absence of HA the hydrodynamic radius of free unimers of Fbg are found at 12 nm. This value is compatible with the size of Fbg molecule at these pH conditions [38]. The R_h of the complexes is between 80 and 90 nm. The detailed values for the size and mass of the four HA-Fbg complexes at pH 4 can be found in Fig. 4 and Fig. 5.

In Fig. 1b the effect of pH on the stability of the electrostatic complexes is illustrated. It is clear that at pH 7.4 the complexes disintegrate, because pH is higher than the pI of Fbg. At pH 7.4 the presence of free Fbg is evident at ~10 nm. A very broad distribution with average R_h in the order of 500–600 nm results from the presence of aggregates of various sizes in solution. The scattered intensity of the solutions at neutral pH is significantly lower than the one at pH 4 (not shown). This shows that most of the complexes are dissolved. Conclusively at neutral pH, complexes are diminished and there is no evidence of stable NPs. This has been confirmed for all the four different instances of HA-Fbg complexes.

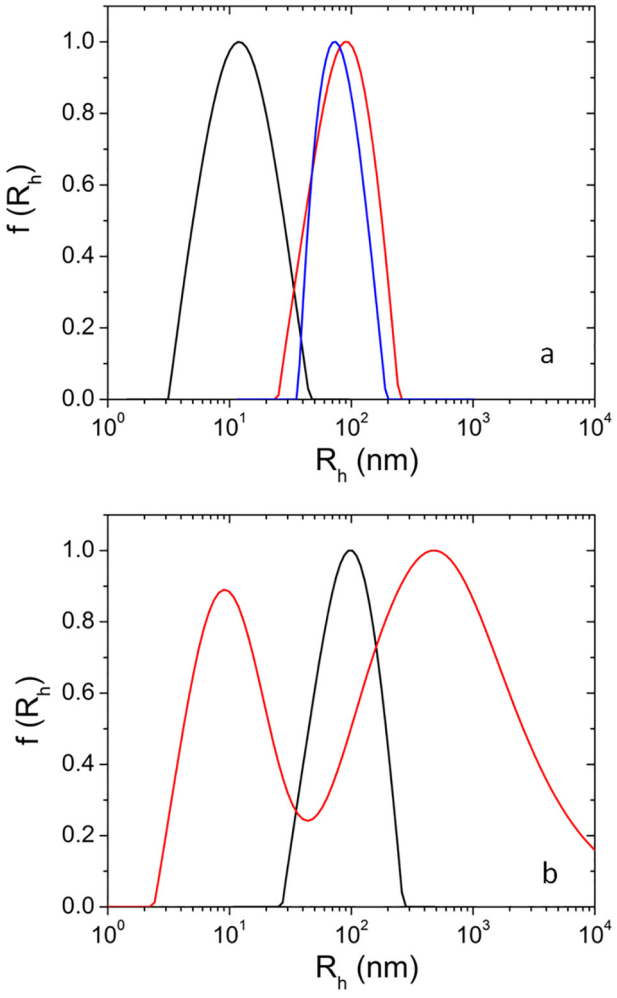

Fig. 1. (a) CONTIN analysis of aqueous solutions of mixtures of HA at 0 (black), 3×10^{-3} (red) and 7×10^{-3} mgml^{-1} (blue) with Fbg at 0.1 mgml^{-1} at pH 4 (scattering angle 90°). (b) CONTIN analysis from complexes at HA/Fbg (3×10^{-3} mgml^{-1}/0.1 mgml^{-1}) at pH 4 (black) and pH 7.4 (red) (scattering angle 90°).

3.2. Stabilization of HA-Fbg NPs by thermal treatment

Denaturation of the secondary structure of Fbg caused by heat treatment in aqueous solutions has been confirmed by atomic force microscopy studies. Fbg molecules are in the trinodular structure (one central globular region and two lateral globular regions) at temperatures up to 45 °C. At temperatures between 65 and 90 °C globular structures surrounded by fibrils are observed. At 90 °C in particular, where the central globular region is still intact ($T_m \approx 94$ °C) while the lateral globules (C terminal region of Aα chains) are melted ($T_m \approx 77$ °C), globular aggregates of a wide size distribution are formed [39]. A possible mechanism of aggregation is that these regions may refold into intermolecular globules causing irreversible intermolecular bridges [39,40]. Temperature-induced aggregation in Fbg solutions has been also confirmed by turbidity measurements at pH ~ 7 where aggregation occurred above 50 °C. Scanning electron microscopy revealed globular structures of heat-denatured Fbg with size about 400 nm [41]. In that case the temperature-induced exposure of haptotactic peptides (haptides) was considered as a main reason of Fbg aggregation. These amphiphilic haptides have been identified in the C-termini of β-chain, extended αE chain and γ-chain and are associated with cell binding and in particular cell adhesion and migration into fibrin clots [42].

In our case, with Fbg concentration at 0.1 mgml^{-1}, application of the thermal protocol on solutions with pure Fbg leads to aggregates of a high degree of polydispersity with very low average apparent molar mass in comparison with HA-Fbg complexes (not shown). Apparently the formation of Fbg aggregates by heat treatment in the absence of HA does not lead to well-defined NPs. The pre-complexation with the polysaccharide offers a neat and controllable way for nanoformulation as it has been previously demonstrated with CS-BSA NPs [20].

We performed the thermal treatment protocol on HA-Fbg complexes in order to test if stable NPs are produced. Indeed, this was the case as the distributions kept their shapes relatively unchanged at neutral pH without dissolving into multiple-size populations (Fig. 2). The effect of thermal treatment and pH increase on the complexes was evaluated also by SLS in order to quantify their radius of gyration R_g and apparent molar mass M. Representative Guinier plots and fittings with Eq. (2) are shown in Fig. 3a. The quadratic formula is used because the plots appear curved. This is an effect of scattering from internal correlations of the complexes, when the inverse radius of gyration R_g falls inside the SLS q-range i.e. $q_{min} > 1/R_g$, or in other words when R_g > 100–200 nm [20]. The q-dependence of the characteristic relaxation Γ (extracted by DLS) is compatible with this effect. At high q internal dynamics of the complexes are probed (Fig. 3b). Therefore, the plots appear curved and a quadratic formula is used (Eq. (3)). However, the non-linearity of the $\Gamma(q^2)$ is also related to the polydispersity of the complexes. In any case, in the chosen range of HA/Fbg mass ratios there is no sign of free species that would appear as single size-population in the DLS data as it was illustrated in the work of Li et al., at very small protein/polyelectrolyte ratios [35]. This indicates that at this mass ratio regime complexes and NPs dominate the mass of the species in solution. Figs. 2 and 3 are examples that represent the behaviour of all complexes tested in this study (the sizes and molar masses of the individual complexes and NPs at the different conditions are discussed in detail in the following).

The formation of stable NPs is confirmed in Fig. 3. The SLS profiles (Guinier plots) do not change dramatically upon change of pH from acidic to neutral conditions. Similar is the case for the relaxation rate. More details are shown in Fig. 4a. The molar mass of the formed complexes at pH 4 shows a marginal increase as a function of HA

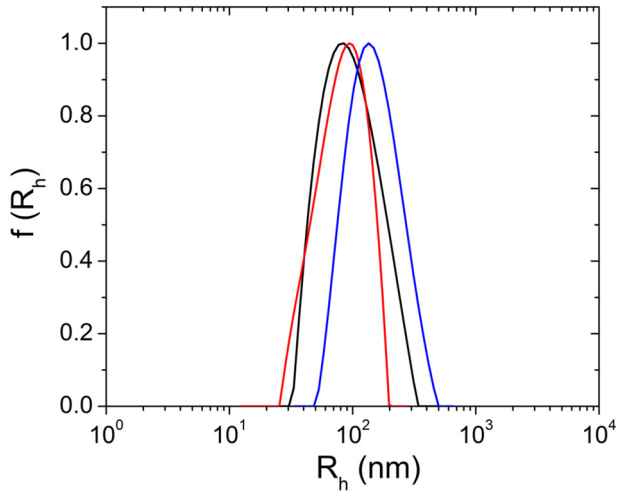

Fig. 2. CONTIN analysis of complexes at HA 5×10^{-3} mgml^{-1} and Fbg 0.1 mgml^{-1}, untreated at pH 4 (black), treated at pH 4 (red) and setting pH to 7.4 after thermal treatment (blue) (scattering angle 90°).

concentration. Thermal treatment causes a small increase in molar mass. The mass increase was also found for the CS-BSA system and was attributed to the addition of free protein that accumulates on the pre-formed complexes [20]. In any case, the NPs keep their integrity upon pH increase while their molar mass slightly increases, contrary to the dramatic mass decrease observed in untreated complexes. The heat-stabilized complexes can therefore be from now on termed as NPs. The increase in M upon pH increase is an opposite trend than the one found in the case of CS-BSA where a mild decrease in molar mass was connected to partial loss of complexed molecules [20]. For solutions of pure Fbg it has been shown that there is a strong tendency for aggregation in a so-called Fbg instability window [37] in the regime 4.5 < pH < 7.5. In solutions of free Fbg a 10-times increase in R_h was observed, however in the case of thermally stabilized HA-Fbg NPs there is only a moderate increase in mass. This is an important observation because in the form of NPs the instability in size and high tendency of aggregation appears to have only weak effects. The surface charge of the NPs inherits the protein charge pH-tunability (Fig. 4b). It is about +10 mV at pH 4 and about −30 at pH 7.4. In more detail, pure Fbg has a ζ_p in the order of +20–25 mV at pH 4. The lower value that we observe for the NPs at pH 4 is due to the complexation with HA that causes partial charge neutralization [37]. At pH 7.4 the surface potential was about −20 mV for aggregates of pure Fbg [37]. In our case, a higher value is found because Fbg has at this pH the same charge sign as HA and therefore the overall charge increases.

The gyration and hydrodynamic radii show a weak increase upon thermal treatment (Fig. 5) which is possibly connected to the accompanying increase in molar mass discussed above. There is a further size increase upon setting pH to 7.4. This could be considered as a signature of swelling that is induced by the change of Fbg net charge from positive to

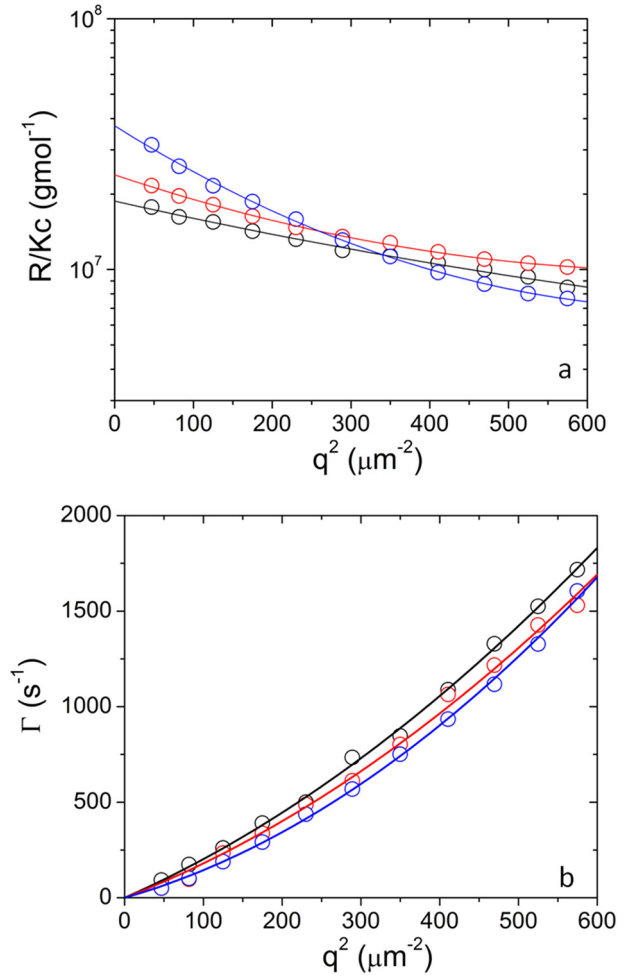

Fig. 3. (a) Guinier plots obtained by SLS (lines are fits with eq. 2) and (b) characteristic relaxation rate obtained by DLS (lines are fits with eq. 3) from HA-Fbg NPs formed at HA 9×10^{-3} mgml^{-1} and Fbg 0.1 mgml^{-1} at pH 4 (black), after thermal treatment at pH 4 (red) and after thermal treatment setting pH to 7.4 (blue).

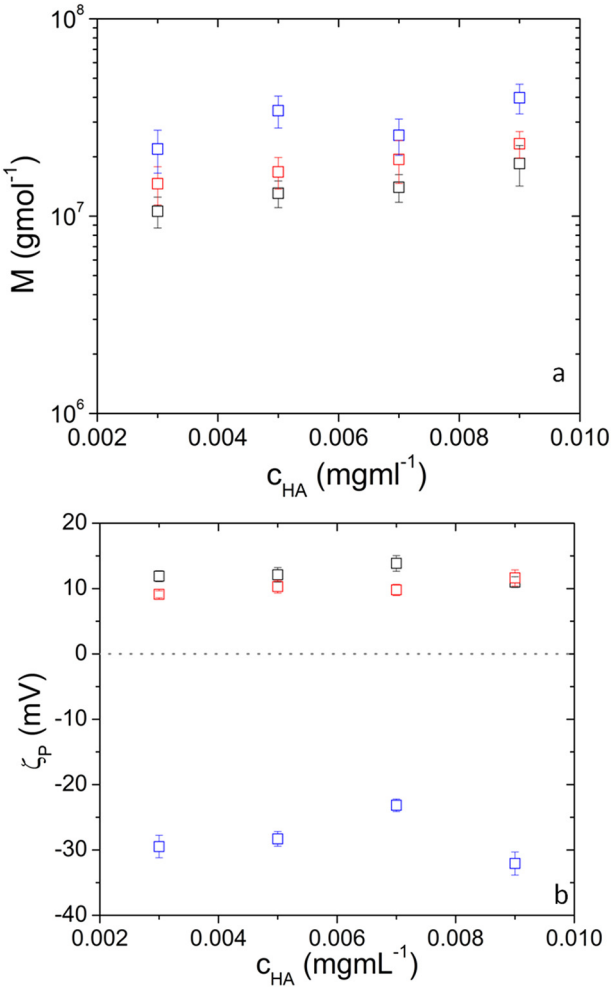

Fig. 4. (a) Molar mass and (b) ζ-potential of HA-Fbg (0.1 mgml^{-1}) NPs at pH 4 (black), after thermal treatment at pH 4 (red) and after thermal treatment setting pH to 7.4 (blue).

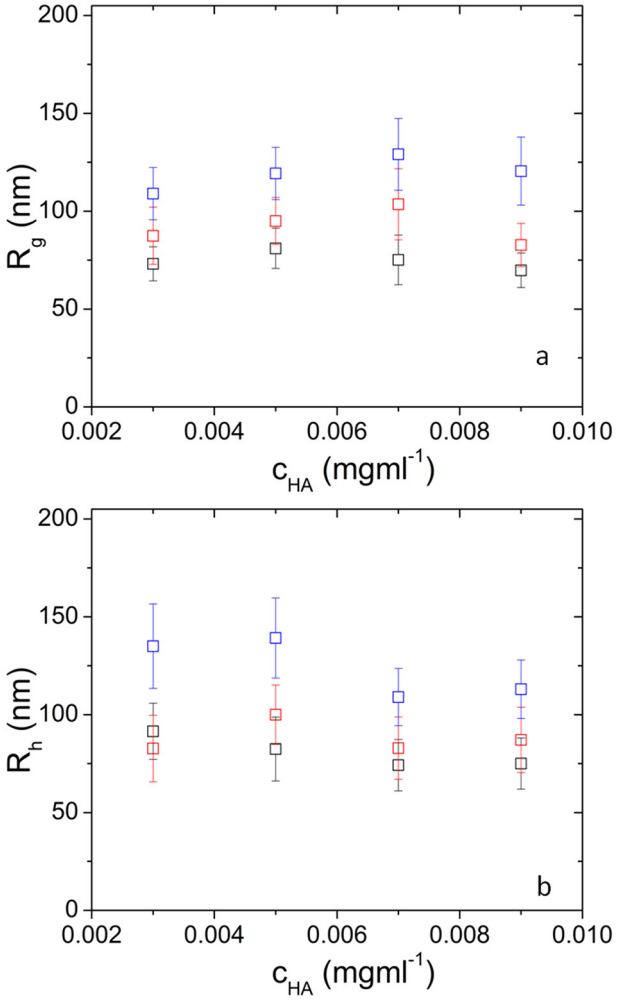

Fig. 5. (a) Radius of gyration and (b) hydrodynamic radius of HA-Fbg NPs at pH 4 (black), after thermal treatment at pH 4 (red) and after thermal treatment setting pH to 7.4 (blue).

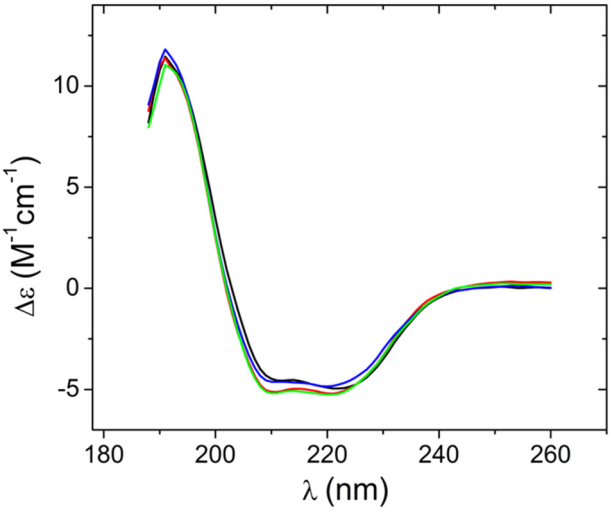

Fig. 6. CD spectra from HA-FBg (5×10^{-3} mgml^{-1}/0.1 mgml^{-1}) solutions at pH 4 (black), at pH 7.4 (red), at pH 4 after thermal treatment (blue) and setting pH 7.4 after thermal treatment (green).

negative and the strong electrostatic interactions between Fbg-Fbg, HA-HA and Fbg—HA molecules. However this swelling effect was stronger in the case of CS-BSA NPs [20]. Additionally, one has to keep in mind that there is an increase in the mass of the NPs. Therefore, we cannot conclude that this size increase is certainly a swelling effect. In any case the NPs are efficiently stable upon pH changes both in size and mass in comparison to untreated electrostatic complexes.

The native conformation of Fbg is crucial for its biofunctions, i.e. cell attachment and blood coagulation, while changes of conformation of Fbg inside NPs may affect their hemocompatibility [43,44]. The secondary structure of Fbg molecules does not show any significant or systematic change upon complexation (not shown) or upon thermal treatment while the characteristic negative bands of the α-helix conformation [45] at 208 and 222 nm are evident (Fig. 6). The analysis of the CD data reveal an α-helix and β-sheet content at 39 ± 4% and 24 ± 3% respectively, which are in agreement with the reported values for native Fbg in aqueous media [40,46]. CD analysis has been performed to all complexes and NPs at the different conditions in order to confirm these results.

3.3. Effect of salt and curcumin-loading on HA-Fbg NPs

In pharmaceutical and food science applications NPs need to perform at environments of increased salinity and often to be loaded with hydrophobic substances. We tested the solution behaviour of our NPs in a wide range of ionic strengths which are relevant to applications. In Fig. 7 the effect of salt on complexes and thermally stabilized NPs is presented by the example of HA-Fbg (5×10^{-3} mgml^{-1}/0.1 mgml^{-1}) NPs.

The apparent molar mass in the solutions of HA-Fbg complexes and NPs increases as a function of salt concentration at pH 4 (Fig. 7a). This signifies inter-particle aggregation which is caused by the screening of electrostatic repulsions and the short-range hydrophobic attractions between Fbg molecules. In the case of pH 7.4 molar mass remains fairly unchanged for the NPs. Their high surface charge (Fig. 4b) keeps the NPs from aggregating. This behaviour is also followed by R_g (Fig. 7b). The aggregation is much more evident in R_h for complexes which shows the high instability of the complexes without thermal treatment (Fig. 7c). The NPs are much less prone to aggregation when they are thermally treated. In DLS the Brownian motion of the whole aggregate is measured and sizes higher than the SLS range (100–200 nm) can be probed. R_h reaches 750 nm in untreated complexes (Fig. 7c). Thermally treated NPs have a greatly enhanced resistance to aggregation in comparison to untreated complexes, especially at pH 7.4 due to their high surface charge.

Fbg has been shown to effectively encapsulate and stabilize curcumin in aqueous media [26]. The encapsulation of curcumin by thermally treated HA-Fbg NPs is illustrated in Fig. 8. The UV–Vis absorbance is unchanged even 48 h after encapsulation of the nutraceutical compound while no sign of precipitation was observed. This means that curcumin remains well-solubilized in the aqueous media by the aid of the NPs. Light scattering experiments were performed on the NPs with encapsulated curcumin. The mass of the NPs slightly increased after curcumin encapsulation, showing that the increased hydrophobic content introduced by the drug induced only weak inter-particle aggregation (not shown). This did not result in a significant increase in the size of the NPs.

4. Conclusions

The ability of Fbg to irreversibly self-assemble upon thermal treatment was utilized to formulate it in NPs using biocompatible components and methods. Complexes between HA and Fbg of well-defined mass and size distribution are created at acidic pH by electrostatic concentration. They are however unstable at neutral pH, as expected, because of the protein's pH-tunable charge. Thermal treatment stabilizes the NPs against pH changes. In the presence of high salt, the NPs have increased stability in size and mass in comparison to untreated complexes. They are also able to solubilize curcumin while the resulting increased hydrophobicity of the NPs causes minor changes to their mass.

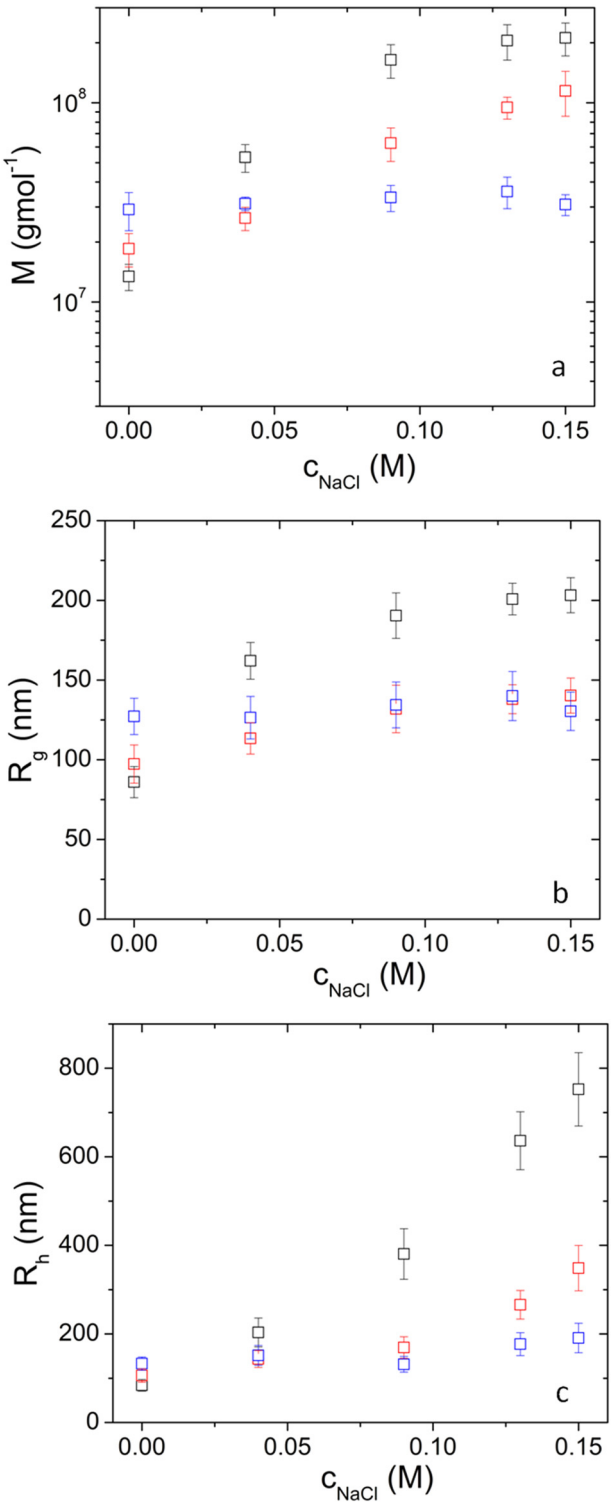

Fig. 7. (a) Molar mass, (b) Radius of gyration and (c) hydrodynamic radius of HA-Fbg (5×10^{-3} mgml^{-1}/0.1 mgml^{-1}) NPs at pH 4 (black), after thermal treatment at pH 4 (red) and after thermal treatment setting pH to 7.4 (blue) as a function of salt content.

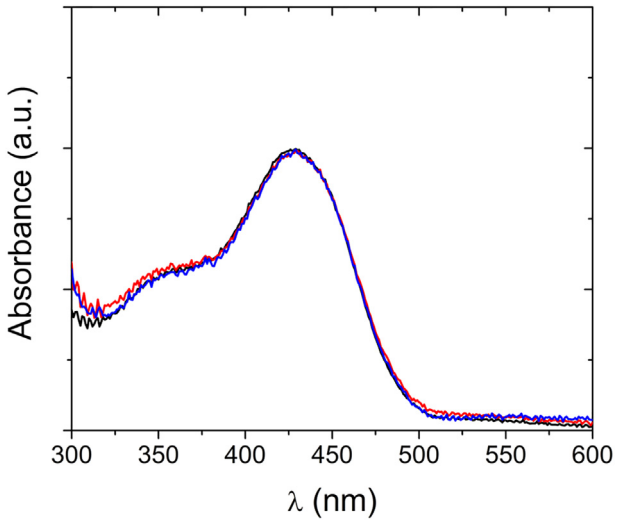

Fig. 8. Curcumin UV–vis absorption spectra in blank aqueous solution (black), in solution of HA-Fbg (7×10^{-3} mgml^{-1}/0.1 mgml^{-1}) NPs (red) and in solution of HA-Fbg (9×10^{-3} mgml^{-1}/0.1 mgml^{-1}) NPs (blue) at pH 4.

These NPs are expected to be useful for applications in drug delivery, tissue engineering and wound healing as they inherit the remarkable multifunctionality of Fbg.

Funding

This research did not receive any specific grant from funding agencies in the public, commercial, or not-for-profit sectors.

CRediT authorship contribution statement

Eleni Vlassi: Validation, Formal analysis, Investigation, Writing - original draft, Writing - review & editing, Visualization. **Aristeidis Papagiannopoulos:** Conceptualization, Methodology, Formal analysis, Writing - original draft, Writing - review & editing, Supervision.

References

[1] A. Jain, S.K. Singh, S.K. Arya, S.C. Kundu, S. Kapoor, Protein nanoparticles: promising platforms for drug delivery applications, ACS Biomaterials Science & Engineering 4 (12) (2018) 3939–3961.
[2] D. Verma, N. Gulati, S. Kaul, S. Mukherjee, U. Nagaich, Protein based nanostructures for drug delivery, J Pharm (Cairo) 2018 (2018) 18 9285854.
[3] L. Yang, F. Cui, D. Cun, A. Tao, K. Shi, W. Lin, Preparation, characterization and biodistribution of the lactone form of 10-hydroxycamptothecin (HCPT)-loaded bovine serum albumin (BSA) nanoparticles, Int. J. Pharm. 340 (1) (2007) 163–172.
[4] K. Langer, S. Balthasar, V. Vogel, N. Dinauer, H. von Briesen, D. Schubert, Optimization of the preparation process for human serum albumin (HSA) nanoparticles, Int. J. Pharm. 257 (1) (2003) 169–180.
[5] W.F. Daamen, J.H. Veerkamp, J.C.M. van Hest, T.H. van Kuppevelt, Elastin as a biomaterial for tissue engineering, Biomaterials 28 (30) (2007) 4378–4398.
[6] Y. Wu, J.A. MacKay, J.R. McDaniel, A. Chilkoti, R.L. Clark, Fabrication of elastin-like polypeptide nanoparticles for drug delivery by electrospraying, Biomacromolecules 10 (1) (2009) 19–24.
[7] J.Y. Oh, H.S. Kim, L. Palanikumar, E.M. Go, B. Jana, S.A. Park, H.Y. Kim, K. Kim, J.K. Seo, S.K. Kwak, C. Kim, S. Kang, J.-H. Ryu, Cloaking nanoparticles with protein corona shield for targeted drug delivery, Nat. Commun. 9 (1) (2018) 4548.
[8] P.L. Lam, S.H.L. Kok, R. Gambari, T.W. Kok, H.Y. Leung, K.L. Choi, C.S. Wong, D.K.P. Hau, W.Y. Wong, K.H. Lam, Z.X. Bian, K.K.H. Lee, C.H. Chui, Evaluation of berberine/bovine serum albumin nanoparticles for liver fibrosis therapy, Green Chem. 17 (3) (2015) 1640–1646.
[9] W. Watcharin, C. Schmithals, T. Pleli, V. Köberle, H. Korkusuz, F. Hübner, O. Waidmann, S. Zeuzem, H.-W. Korf, A. Terfort, S. Gelperina, T.J. Vogl, J. Kreuter, A. Piiper, Detection of hepatocellular carcinoma in transgenic mice by Gd-DTPA- and rhodamine 123-conjugated human serum albumin nanoparticles in T1 magnetic resonance imaging, J. Control. Release 199 (2015) 63–71.
[10] A. Papagiannopoulos, A. Meristoudi, S. Pispas, A. Radulescu, Micelles from HOOC-PnBA-b-PAA-C12H15 diblock amphiphilic polyelectrolytes as protein nanocarriers, Biomacromolecules 17 (11) (2016) 3816–3827.
[11] Y.Q. Yang, L.S. Zheng, X.D. Guo, Y. Qian, L.J. Zhang, pH-sensitive micelles self-assembled from amphiphilic copolymer brush for delivery of poorly water-soluble drugs, Biomacromolecules 12 (1) (2011) 116–122.
[12] W.C. Blocher, S.L. Perry, Complex coacervate-based materials for biomedicine, WIREs Nanomedicine and Nanobiotechnology 9 (4) (2017), e1442. .
[13] C.L. Cooper, P.L. Dubin, A.B. Kayitmazer, S. Turksen, Polyelectrolyte–protein complexes, Curr. Opin. Colloid Interface Sci. 10 (1) (2005) 52–78.
[14] F. Comert, A.J. Malanowski, F. Azarikia, P.L. Dubin, Coacervation and precipitation in polysaccharide-protein systems, Soft Matter 12 (18) (2016) 4154–4161.
[15] O.G. Jones, E.A. Decker, D.J. McClements, Comparison of protein–polysaccharide nanoparticle fabrication methods: impact of biopolymer complexation before or after particle formation, J. Colloid Interface Sci. 344 (1) (2010) 21–29.

[16] O.G. Jones, D.J. McClements, Biopolymer nanoparticles from heat-treated electrostatic protein–polysaccharide complexes: factors affecting particle characteristics, J. Food Sci. 75 (2) (2010) N36–N43.
[17] R. Wetzel, M. Becker, J. Behlke, H. Billwitz, S. Böhm, B. Ebert, H. Hamann, J. Krumbiegel, G. Lassmann, Temperature behaviour of human serum albumin, Eur. J. Biochem. 104 (2) (1980) 469–478.
[18] F.J. Gutiérrez, S.M. Albillos, E. Casas-Sanz, Z. Cruz, C. García-Estrada, A. García-Guerra, J. García-Reverter, M. García-Suárez, P. Gatón, C. González-Ferrero, I. Olabarrieta, M. Olasagasti, S. Rainieri, D. Rivera-Patiño, R. Rojo, A. Romo-Hualde, M.-J. Sáiz-Abajo, M.-L. Mussons, Methods for the nanoencapsulation of β-carotene in the food sector, Trends Food Sci. Technol. 32 (2) (2013) 73–83.
[19] N. Ron, P. Zimet, J. Bargarum, Y.D. Livney, Beta-lactoglobulin–polysaccharide complexes as nanovehicles for hydrophobic nutraceuticals in non-fat foods and clear beverages, Int. Dairy J. 20 (10) (2010) 686–693.
[20] A. Papagiannopoulos, E. Vlassi, Stimuli-responsive nanoparticles by thermal treatment of bovine serum albumin inside its complexes with chondroitin sulfate, Food Hydrocoll. 87 (2019) 602–610.
[21] S. Kattula, J.R. Byrnes, A.S. Wolberg, Fibrinogen and fibrin in hemostasis and thrombosis, Arterioscler. Thromb. Vasc. Biol. 37 (3) (2017) e13–e21.
[22] S. Kalasin, M.M. Santore, Non-specific adhesion on biomaterial surfaces driven by small amounts of protein adsorption, Colloids Surf. B: Biointerfaces 73 (2) (2009) 229–236.
[23] S.A. Sell, M.P. Francis, K. Garg, M.J. McClure, D.G. Simpson, G.L. Bowlin, Cross-linking methods of electrospun fibrinogen scaffolds for tissue engineering applications, Biomed. Mater. 3 (4) (2008), 045001. .
[24] S. Huang, C. Wang, J. Xu, L. Ma, C. Gao, In situ assembly of fibrinogen/hyaluronic acid hydrogel via knob-hole interaction for 3D cellular engineering, Bioactive Materials 2 (4) (2017) 253–259.
[25] T. Rajangam, S.S.A. An, Fibrinogen and fibrin based micro and nano scaffolds incorporated with drugs, proteins, cells and genes for therapeutic biomedical applications, Int. J. Nanomedicine 8 (2013) 3641–3662.
[26] M.H.M. Leung, T.W. Kee, Effective stabilization of curcumin by association to plasma proteins: human serum albumin and fibrinogen, Langmuir 25 (10) (2009) 5773–5777.
[27] N.S. Rejinold, M. Muthunarayanan, N. Deepa, K.P. Chennazhi, S.V. Nair, R. Jayakumar, Development of novel fibrinogen nanoparticles by two-step co-acervation method, Int. J. Biol. Macromol. 47 (1) (2010) 37–43.
[28] N.S. Rejinold, M. Muthunarayanan, K.P. Chennazhi, S.V. Nair, R. Jayakumar, Curcumin loaded fibrinogen nanoparticles for cancer drug delivery, J. Biomed. Nanotechnol. 7 (4) (2011) 521–534.
[29] N.S. Rejinold, T. Baby, K.P. Chennazhi, R. Jayakumar, Dual drug encapsulated thermosensitive fibrinogen-graft-poly (N-isopropyl acrylamide) nanogels for breast cancer therapy, Colloids Surf. B: Biointerfaces 114 (2014) 209–217.
[30] B. Chu, Laser Light Scattering, 2 ed. Academic Press, New York, 1991.
[31] A. Papagiannopoulos, Bovine serum albumin interactions with cationic surfactant vesicles decorated by a low-molar-mass polysaccharide, Colloids Surf. A Physicochem. Eng. Asp. 537 (2018) 495–501.
[32] B.J. Berne, R. Pecora, Dynamic Light Scattering, With Applications to Chemistry, Biology, and Physics, Dover, Toronto, 2000.
[33] A. Micsonai, F. Wien, L. Kernya, Y.-H. Lee, Y. Goto, M. Réfrégiers, J. Kardos, Accurate secondary structure prediction and fold recognition for circular dichroism spectroscopy, Proc. Natl. Acad. Sci. 112 (24) (2015) E3095–E3103.
[34] A.B. Kayitmazer, D. Seeman, B.B. Minsky, P.L. Dubin, Y. Xu, Protein-polyelectrolyte interactions, Soft Matter 9 (9) (2013) 2553–2583.
[35] Y. Li, K.W. Mattison, P.L. Dubin, H.A. Havel, S.L. Edwards, Light scattering studies of the binding of bovine serum albumin to a cationic polyelectrolyte, Biopolymers 38 (4) (1996) 527–533.
[36] H. Matsunami, R. Kikuchi, K. Ogawa, E. Kokufuta, Light scattering study of complex formation between protein and polyelectrolyte at various ionic strengths, Colloids Surf. B: Biointerfaces 56 (1) (2007) 142–148.
[37] M. Wasilewska, Z. Adamczyk, B. Jachimska, Structure of fibrinogen in electrolyte solutions derived from dynamic light scattering (DLS) and viscosity measurements, Langmuir 25 (6) (2009) 3698–3704.
[38] Z. Adamczyk, B. Cichocki, M.L. Ekiel-Jeżewska, A. Słowicka, E. Wajnryb, M. Wasilewska, Fibrinogen conformations and charge in electrolyte solutions derived from DLS and dynamic viscosity measurements, J. Colloid Interface Sci. 385 (1) (2012) 244–257.
[39] N.A. Barinov, A.D. Protopopova, E.V. Dubrovin, D.V. Klinov, Thermal denaturation of fibrinogen visualized by single-molecule atomic force microscopy, Colloids Surf. B: Biointerfaces 167 (2018) 370–376.
[40] N. Hassan, L.R.S. Barbosa, R. Itri, J.M. Ruso, Fibrinogen stability under surfactant interaction, J. Colloid Interface Sci. 362 (1) (2011) 118–126.
[41] G. Marx, X. Mou, A. Hotovely-Salomon, L. Levdansky, E. Gaberman, D. Belenky, R. Gorodetsky, Heat denaturation of fibrinogen to develop a biomedical matrix, J. Biomed. Mater. Res. B Appl. Biomater. 84B (1) (2008) 49–57.
[42] R. Gorodetsky, A. Vexler, M. Shamir, J. An, L. Levdansky, I. Shimeliovich, G. Marx, New cell attachment peptide sequences from conserved epitopes in the carboxy termini of fibrinogen, Exp. Cell Res. 287 (1) (2003) 116–129.
[43] A.S. Zhao, S. Zhou, Y. Wang, J. Chen, C.R. Ye, N. Huang, Molecular interaction of fibrinogen with thermally modified titanium dioxide nanoparticles, RSC Adv. 4 (76) (2014) 40428–40434.
[44] W. Zhang, D. Zhong, Q. Liu, Y. Zhang, N. Li, Q. Wang, Z. Liu, W. Xue, Effect of chitosan and carboxymethyl chitosan on fibrinogen structure and blood coagulation, J. Biomater. Sci. Polym. Ed. 24 (13) (2013) 1549–1563.
[45] Kenry, K.P. Loh, C.T. Lim, Molecular interactions of graphene oxide with human blood plasma proteins, Nanoscale 8 (17) (2016) 9425–9441.
[46] Y. Chen, H. Mao, X. Zhang, Y. Gong, N. Zhao, Thermal conformational changes of bovine fibrinogen by differential scanning calorimetry and circular dichroism, Int. J. Biol. Macromol. 26 (2–3) (1999) 129–134.